Lattice-constant and electron-affinity effects on negative-ion conversion in atom–ionic-crystal-surface grazing scattering

Wang Zhou, Hu Zhou,* Meixiao Zhang, Lihua Zhou, Yuan Li, Bowen Li, and Ximeng Chen*
School of Nuclear Science and Technology, Lanzhou University, Lanzhou 730000, China
(Received 29 July 2016; published 29 November 2016)

The effects of the lattice constant and electron affinity on the negative-ion conversion of a neutral atom undergoing grazing scattering on an ionic-crystal surface over the complete velocity range were investigated. Here, a comparison of negative-ion conversion of neutral O^0-KCl(100),F^0-KCl(100), and O^0-KI(100) surface systems shows that the pronounced difference in the efficiency of negative-ion formation between F^0-KCl(100) and O^0-KCl(100) is caused by the large difference in their projectile electron affinities, whereas the difference between O^0-KI(100) and O^0-KCl(100) is caused by the difference in their lattice constants.

DOI: 10.1103/PhysRevA.94.052708

I. INTRODUCTION

The electron-transfer process plays an important role in surface reactions. The interaction of an atom or an ion with a metal surface [1–5] and a cluster [6,7] is explained by the resonant electron-transfer process, which has been demonstrated previously [8–12]. However, for dielectric surfaces, experimental and theoretical studies [13–19] on ionic insulator (oxide and alkali-metal halide) surfaces have demonstrated that their behavior is distinct from that of metals. For metals, charge transfer is generally described by a jellium model [1–12], and resonant electron-transfer processes are well understood within this approximation [4,12]. However, for ionic solids, the localized property of alternate positive and negative charges requires a different description that involves a nonresonant electron-transfer [13–16] process. Compared with the image shift at a metal surface, the Madelung potential plays a key role in the specific energy level shift of atomic states near the surface [20]. Despite a variety of theoretical works on the related negative-ion conversion mechanism, this process is not yet adequately understood. One representative characteristic is the unexpectedly high fraction of negative-ion conversions for atoms under grazing scattering on an ionic-crystal surface [21]. Recently, we proposed a simple analytical model for the entire velocity range of negative-ion formation on a typical AB-type ionic-crystal surface by grazing scattering of natural atoms [22], and we demonstrated the effects of image interaction, Mott-Littleton polarization interaction, and effective crossing number N on the final negative-ion formation.

Negative-ion conversion of neutral atoms on an insulating ionic-crystal surface can be directly applied (1) to the design of low-flux negative-ion beam sources [16], and (2) in space research for the construction of neutral particle detectors [23]. The key step for these techniques is to choose the suitable projectile-surface combinations that have a small electron-capture energy defect and a small negative-ion detachment probability. The electron affinity and the lattice constant were generally being viewed as two directly important characteristic parameters for a projectile-target combination. Investigation of their influence on the final negative-ion formation has important practical significance. In this work, we demonstrate the difference between the contributions of the lattice constant and electron affinity to the negative-ion conversion of neutral atoms for various projectile–ionic-crystal-surface systems. The results are based on negative-ion formation on two alkali-metal halide crystal surfaces as shown in previous experiments.

In this study, we considered F^0_{gas}-KCl(100), O^0_{gas}-KCl(100), and O^0_{gas}-KI(100) surface systems for three reasons. (1) Experimental data regarding the yields of F^- and O^- ions under grazing scattering of neutral atoms from KCl(100) and the yields of O^- ions formed on KI(100) surfaces are available [21]. (2) Significant differences occur in the electron affinity between F^- ($\varepsilon_{F^-} = 3.4$ eV [24]) and O^- ($\varepsilon_{O^-} = 1.46$ eV [24]) ions. (3) Valence and conduction bands of the two crystals show a similar structure and produce small differences [16].

This paper is organized as follows. In Sec. II, we briefly recall the theoretical model and the contributions of three interactions [point-charge (PC) energy defect, Mott-Littleton (ML) polarization interaction, and image interaction] to the electron-capture energy defect. In Sec. III, we present the detailed calculation results, which focus on the actual electron-capture energy defect (Sec. III A) and the single-collision negative-ion conversion probability (Sec. III B). In Sec. IV, we summarize the conclusions. Atomic units are used unless otherwise stated.

II. ELECTRON-CAPTURE ENERGY DEFECT

A. Theoretical models

The alkali-metal halide ionic crystal has alternating $+1$ and -1 charges distributed at the lattice sites of Alk^+ and Hal^-, respectively. For neutral A^0_{gas} projectiles undergoing grazing scattering along the ⟨100⟩ direction of KCl(100) and KI(100) surfaces (shown in Fig. 1), the trajectories are a result of small-angle scattering of projectiles with a large number of ions in the surface plane, and they are nearly identical for all projectiles [13]. The valence band of alkali-metal halide originates from the $Hal^-(np_{x,y,z})$ orbitals, and the valence-band electrons are localized at the Hal^- sites [25]. Electron capture of a projectile A^0_{gas} from the surface of an alkali-metal halide ionic crystal is closely related to the localized valence-band electrons. Therefore, a series of sequential binary collisions of

*zhouhu19860224@163.com and chenxm@lzu.edu.cn

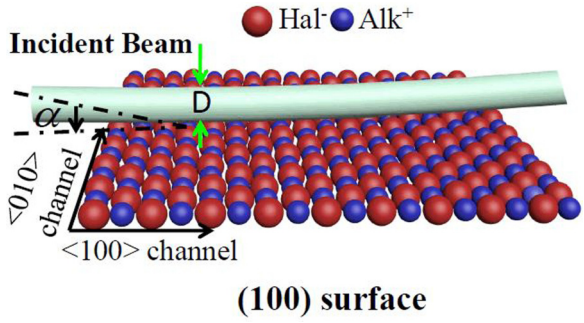

FIG. 1. Sketch of the A^0_{gas} projectile undergoing grazing scattering from an ionic-crystal surface [here, KCl(100) or KI(100)], where α and D represent the incident angle and diameter of the beam, respectively. The direction of the beam is parallel to the $\langle 100\rangle$ surface axis channel.

the projectile with Hal^- ions at the crystal surface treatment is used here [26].

For the electron-capture reaction of a single collision,

$$A^0_{gas} + Hal^-_{active\ site} \rightarrow A^-_{gas} + Hal^0_{active\ site}. \quad (1)$$

From Ref. [22], the key electron-capture energy defect between the initial $(A^0_{gas} + Hal^-_{active\ site})$ and final $(A^-_{gas} + Hal^0_{active\ site})$ states can be expressed as follows:

$$\Delta E(\mathbf{R}, v) = \Delta E_{PC}(\mathbf{R}) + P_{ML}(\mathbf{R}) + U_{image}(Z, v), \quad (2)$$

Equation (2) implies that the electron-capture energy defect $\Delta E(\mathbf{R},v)$ is composed of three parts: (1) the PC-energy defect $\Delta E_{PC}(\mathbf{R}) = \varepsilon_{Hal^-_{active\ site}} - \varepsilon_{A^-_{gas}} + \{E_M(|\mathbf{R}| = 0) - E_M(\mathbf{R})\}$, where $\varepsilon_{Hal^-_{active\ site}}$ and $\varepsilon_{A^-_{gas}}$ are the electron affinities in the free $Hal^-_{active\ site}$ and A^-_{gas} ions, respectively, where the terms in the bracket are the Madelung potential created by the point charges at the $Hal^-_{active\ site}$ $[E_M(|\mathbf{R}| = 0)]$ and that at the point $\mathbf{R}[E_M(\mathbf{R})]$, and $\mathbf{R} = \{X, Y, Z\}$ is the position vector of the projectile relative to the $Hal^-_{active\ site}$; (2) the ML polarization interaction $P_{ML}(\mathbf{R})$; and (3) the image interaction $U_{image}(Z,v)$. Note that (2) and (3) are both produced by the field polarization of the crystal in the final state of electron capture [27,28].

B. PC-energy defect $\Delta E_{PC}(\mathbf{R})$

The F^0_{gas}-KCl(100), O^0_{gas}-KCl(100), and O^0_{gas}-KI(100) systems, such as in Ref. [22], behave as $\langle \Delta E_{PC}(X,Y,Z)\rangle_{S_0} = \frac{1}{S_0}\iint_{S_0} \Delta E_{PC}(X,Y,Z)dXdY$ and $\Delta E_{PC}(X = Y = 0, Z)$ as shown in Fig. 2 by different types of lines. The same conclusion of the approximation of ΔE_{PC} in S by $\Delta E_{PC}(X = Y = 0, Z)$ is obtained, where $S = \{-a/4 \leqslant X \leqslant a/4, -a/4 \leqslant Y \leqslant a/4\}$ (a is the lattice constant) indicates the effective $Hal^-_{active\ site}$ area and $S_0 = \{-(\frac{a}{4} - r_{A^0_{gas}}) \leqslant X \leqslant (\frac{a}{4} - r_{A^0_{gas}}),\ -(\frac{a}{4} - r_{A^0_{gas}}) \leqslant Y \leqslant (\frac{a}{4} - r_{A^0_{gas}})\}$, where $r_{A^0_{gas}}$ is the radius of the projectile. The actual electron-capture energy defect in the $Hal^-_{active\ site}$ scale of S is the energy defect in S_0. In addition, the comparison reveals that (1) the PC-energy defect $[\Delta E^{ave}_{PC}(Z)$ or $\Delta E_{PC}(X = Y = 0, Z)\ ]$ linearly increases with Z; (2) $0.5\ eV \leqslant \Delta E^{O\text{-}KCl}_{PC} - \Delta E^{O\text{-}KI}_{PC} \leqslant 0.8\ eV$ because of the differences in the lattice constants; (3) large electron affinity

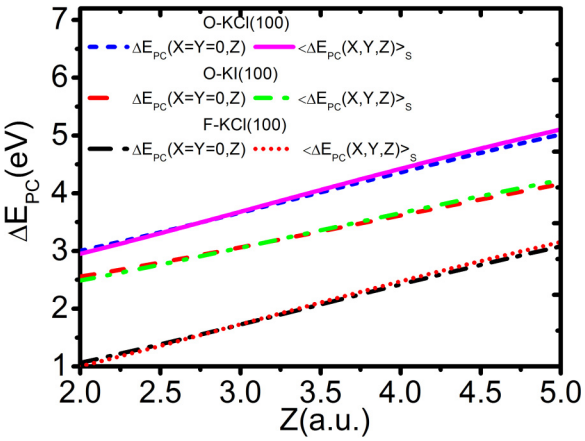

FIG. 2. Both $\Delta E^{ave}_{PC}(Z) = \langle \Delta E_{PC}(X,Y,Z)\rangle_S = \langle \Delta E_{PC}(X,Y,Z)\rangle_{S_0}$ and $\Delta E_{PC}(X = Y = 0, Z)$ as a function of the surface altitude Z are displayed by different types of lines for O^0_{gas}-KCl(100), F^0_{gas}-KCl(100), and O^0_{gas}-KI(100) systems, respectively.

differences lead to $\Delta E^{O\text{-}KCl}_{PC} - \Delta E^{F\text{-}KCl}_{PC} = \varepsilon_{F^-} - \varepsilon_{O^-} = 1.94\ eV$.

C. ML polarization contribution $P_{ML}(\mathbf{R})$

The ML polarization effect correction for the final $(A^-_{gas} + Hal^0_{active\ site})$ state electron-capture energy defect can be obtained from Refs. [16,26], and the anion and cation polarizations of $\alpha_{K^+} = 8.9604$ a.u. and $\alpha_{Cl^-} = 19.8822$ a.u. for KCl and $\alpha_{K^+} = 8.9604$ a.u. and $\alpha_{I^-} = 43.1967$ a.u. for KI are obtained from Ref. [29]. Because of the symmetry of $P_{ML}(-X,Y,Z) = P_{ML}(X,-Y,Z) = P_{ML}(X,Y,Z)$, only $P_{ML}(\mathbf{R})$ in the area of $\{0 \leqslant X \leqslant \frac{a}{4},\ 0 \leqslant Y \leqslant \frac{a}{4}\}$ with different altitudes ($Z = 3.0, 3.5, 4.0$, and 4.5 a.u.) are presented in Figs. 3(a)–3(d) for O^-_{gas}-KCl and F^-_{gas}-KCl. The figure shows that $-1.0 \leqslant P_{ML}(\mathbf{R}) \leqslant -0.3$ eV for Z values between 3.0 and 4.5 a.u. The average of $P_{ML}(\mathbf{R})$ over X, Y in S

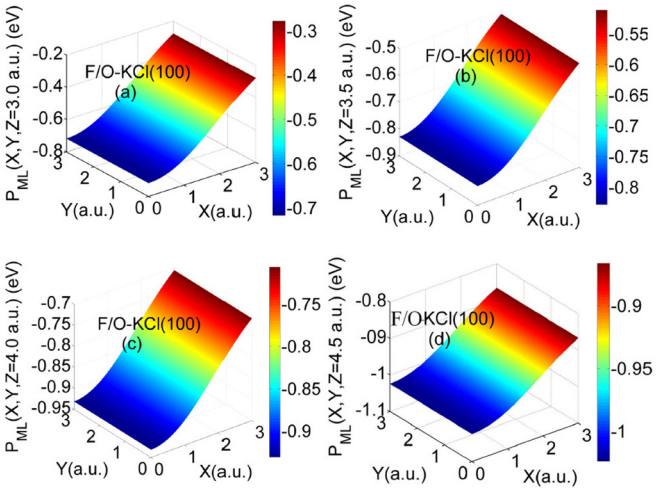

FIG. 3. (a–d) ML polarization contributions $P_{ML}(\mathbf{R})$ of F^0_{gas}-KCl(100) and O^0_{gas}-KCl(100) within the surface $Hal^-_{active\ site}$(here $Cl^-_{active\ site}$) scale S at the projectile-surface altitudes of $Z = 3.0, 3.5, 4.0$, and 4.5 a.u., respectively.

TABLE I. Image interaction parameters.

	ε_∞	$\omega_1(\mathrm{cm}^{-1})$	$\omega_2(\mathrm{cm}^{-1})$	$4\pi\rho_1$	$4\pi\rho_1$	γ_1/ω_1	γ_1/ω_1
KI	2.7[a]	102[a]	316[a]	2.136[a]	0.276[a]	0.084[a]	0.3[a]
KCl	2.22[b]	189.5[b]	210.5[b]	0.0842[b]	0.0379[b]	0.1636[b]	0.0689[b]

[a]Reference [30].
[b]Reference [32].

is $\langle P_{\mathrm{ML}}(X,Y,Z)\rangle_S = \frac{1}{S}\iint_S P_{\mathrm{ML}}(X,Y,Z)dXdY$, $-0.95\,\mathrm{eV} \leqslant \langle P_{\mathrm{ML}}(X,Y,Z)\rangle_S \leqslant -0.5\,\mathrm{eV}$ for Z values between 3.0 and 4.5 a.u. This average is nearly equivalent to the range of $-1.1\,\mathrm{eV} \leqslant \langle P_{\mathrm{ML}}(X,Y,Z)\rangle_S \leqslant -0.6\,\mathrm{eV}$ for O^-_{gas}-KI and F^-_{gas}-KI [22].

D. Image interaction contribution $U_{\mathrm{image}}(Z,v)$

The image interaction that occurs in the final $(A^-_{gas} + Hal^0_{active\ site})$ state can be obtained by the surface response presented in Ref. [30] with the two-oscillator dielectric constant model [31]. The parameters required for the studied systems are shown in Table I.

The calculated image interaction as a function of the projectile's incident velocity v and surface altitude Z for O^0_{gas}-KCl(100), F^0_{gas}-KCl(100), and O^0_{gas}-KI(100) collision systems are displayed in Figs. 4(a) and 4(c), respectively. For $v < 0.08$ a.u. the small vertical energy component $E_\perp$ $[E_\perp^{F^0_{gas}}(v < 0.08\,\mathrm{a.u.}) < 0.925\,\mathrm{eV}, E_\perp^{O^0_{gas}}(v < 0.08\,\mathrm{a.u.}) < 0.779\,\mathrm{eV}]$ should lead to a large closest-approach distance of Z, which is not in the range of $2.0\,\mathrm{a.u.} \leqslant Z \leqslant 4.0\mathrm{a.u.}$. Figures 4(b) and 4(c) present the projection of $U_{\mathrm{image}}(Z,v)$ in the velocity range of $v \geqslant 0.08$ a.u. to four different surface altitudes of $Z = 2.5, 3.0, 3.5$, and 4.0 a.u. for the studied systems. The magnitude of the image interaction $U_{\mathrm{image}}(Z,v)$ decreases as Z increases and increases as the projectile velocity v decreases within the focal range of $v \geqslant 0.08$ a.u.

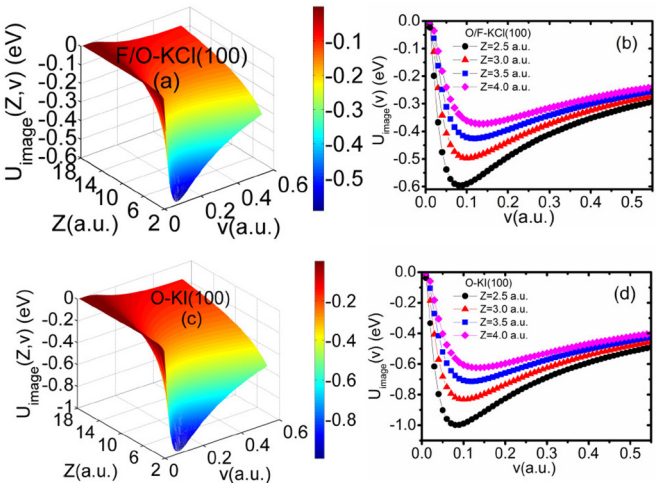

FIG. 4. (a) Three-dimensional plot of U_{image} as a function of both the surface altitude Z and projectile velocity v. (b) U_{image} as a function of the projectile velocity v for fixed surface altitudes of $Z = 2.5, 3.0, 3.5$, and 4.0 a.u. Panels (c,d) are similar to panels (a,b), respectively, except they display the O-KI(100) case.

III. RESULTS AND DISCUSSION

A. Electron-capture energy defect

Considering the ML polarization and image interaction corrections presented above, the average energy defect $\Delta E_{\mathrm{ave}}(Z,v)$ on the scale S of surface $Hal^-_{active\ site}$ (here, Cl^- or I^-) can be expressed as follows [22]:

$$\Delta E_{\mathrm{ave}}(Z,v) \approx \Delta E_{\mathrm{PC}}(X = Y = 0, Z) + \langle P_{\mathrm{ML}}(X,Y,Z)\rangle_S + U_{\mathrm{image}}(Z,v), \quad (3)$$

where $\Delta E_{\mathrm{PC}}(X = Y = 0, Z)$ is the PC-energy defect at $(X = Y = 0, Z)$ point, $\langle P_{\mathrm{ML}}(X,Y,Z)\rangle_S$ is the average ML polarization interaction, and $U_{\mathrm{image}}(Z,v)$ is the image interaction. Figures 5(a)–5(f) display the results calculated from Eq. (3).

The energy differences $\Delta E_{\mathrm{ave}}(Z,v)$ of the electron transfer in the O^0_{gas}-KCl(100), O^0_{gas}-KI(100), and F^0_{gas}-KCl(100) systems are displayed in Figs. 5(a) and 5(b), 5(c) and 5(d), and 5(e) and 5(f), respectively. The electron-transfer energy defect

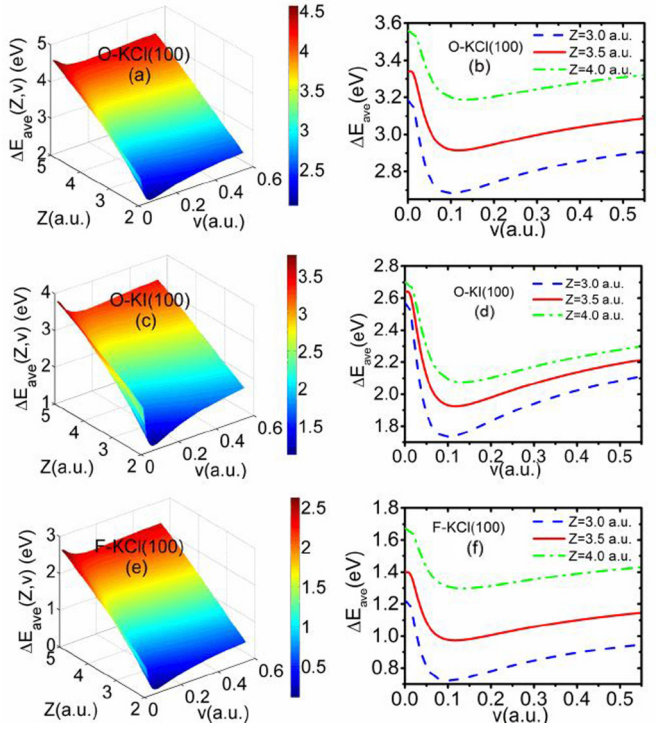

FIG. 5. (a,c,e) Calculated average energy defects $\Delta E_{\mathrm{ave}}(Z,v)$ on the scale S of the surface $Hal^-_{active\ site}$(Cl^- or I^-) as a function of the surface altitude Z and projectile velocity v for the O^0_{gas}-KCl(100), O^0_{gas}-KI(100), and F^0_{gas}-KCl(100) cases, respectively. (b,d,f) $\Delta E_{\mathrm{ave}}(Z,v)$ as a function of the projectile velocity v for fixed surface altitudes of $Z = 3.0, 3.5$, and 4.0 a.u. for the three studied cases, respectively.

$\Delta E_{\rm ave}(Z,v)$ increases rapidly with Z. This characteristic is illustrated in Figs. 5(b), 5(d), and 5(f) where the results are presented for different Z values ($Z = 3.0, 3.5$, and 4.0 a.u.) and the systems $O^0_{\rm gas}$-KCl(100), $O^0_{\rm gas}$-KI(100), and $F^0_{\rm gas}$-KCl(100).

The electron-capture energy defect $\Delta E_{\rm ave}(Z,v)$ is smaller in the $O^0_{\rm gas}$-KI(100) case than in the $O^0_{\rm gas}$-KCl(100) case because the lattice constant of the KI crystal ($a = 13.34$ a.u. [21]) is larger than that of KCl($a = 11.9$ a.u. [21]). Equation (2) implies that the PC-energy defect $\Delta E_{\rm PC}(\mathbf{R})$ is governed by the difference between the Madelung potentials at the active sites and at the position $\mathbf{R}$ of the projectile. Considering the characteristic size of the variation of the Madelung field is determined by the lattice constant a, a smaller ratio of R/a corresponds to a smaller difference in the brackets and a smaller contribution of $\Delta E_{\rm PC}(\mathbf{R})$ (see Fig. 2) to $\Delta E(\mathbf{R},v)$. Although image interaction $U_{\rm image}(Z,v)$ (Fig. 4) and ML polarization interaction $P_{\rm ML}(\mathbf{R})$ (Fig. 3) each substantially reduce the energy defect $\Delta E_{\rm ave}(Z,v)$, the comparable magnitude between both cases indicates that they play a negligible role in the difference; therefore, the projectile velocity dependence of $\Delta E_{\rm ave}(Z,v)$ is dependent on the image interaction.

The smaller $\Delta E_{\rm ave}(Z,v)$ energy differences in the $F^0_{\rm gas}$-KCl(100) case compared to the $O^0_{\rm gas}$-KCl(100) case are caused by the electron affinity of free $F^-_{\rm gas}$ ($\varepsilon_{F^-_{\rm gas}} = 3.4$ eV) [24], which is more than two times larger than that of free $O^-_{\rm gas}$ ($\varepsilon_{O^-_{\rm gas}} = 1.46$ eV) [24].

B. Single-collision negative-ion conversion

For a single-collision negative-ion conversion of the incident atom with the surface $\rm Hal^-_{active\ site}$, by considering the trajectory statistics, the final probability of the negative-ion conversion can be obtained by $P^{\rm site}_{\rm S}(Z,v) = 2P^{\rm site}_{\rm cap}(Z,v)[1 - P_{\rm det}(v)]$, where the electron-capture probability $P^{\rm site}_{\rm cap}(Z,v)$ for neutral projectiles from the surface $\rm Hal^-_{active\ site}$ is obtained from Ref. [21] with the calculated energy defect from Eq. (3). $P_{\rm det}(v)$ represents the affinity electron detachment probability. For an affinity electron detachment, we consider the Coulomb tunneling loss during the $A^-_{\rm gas}$ ($F^-_{\rm gas}$ or $O^-_{\rm gas}$) ion interactions with a surface $\rm Hal^-_{site}$($Cl^-_{\rm site}$or $I^-_{\rm site}$), which is further discussed in Ref. [22]. The nonscreened Coulomb potential and the corresponding calculated detachment probabilities of $F^-_{\rm gas}$ (red solid line) and $O^-_{\rm gas}$ (blue dashed line) ions are displayed in Figs. 6(g) and 6(h), respectively. $P^{\rm site}_{\rm S}(Z,v)$ represents the negative-ion conversion probability of a neutral projectile lying in the (X,Y) plane at a distance Z from the surface. Thus, the negative-ion conversion probability for crossing a row of surface ions oriented along the $\langle 010\rangle$ channeling direction (vertical to the beam traveling direction of $\langle 100\rangle$) is $P^{\rm row}_{\rm S}(Z,v) = \frac{1}{2}P^{\rm site}_{\rm S}(Z,v)$.

Figures 6(a), 6(c), and 6(e) display the relationship of $P^{\rm site}_{\rm S}(Z,v)$ with Z and v for $O^0_{\rm gas}$-KCl(100), $O^0_{\rm gas}$-KI(100), and $F^0_{\rm gas}$-KCl(100) systems, respectively. Figures 6(b), 6(d), and 6(f) show the projectile velocity dependence of the negative-ion conversion probability [$P^{\rm site}_{\rm S}(Z,v)$] in a single binary collision for four representative values: $Z = 3.0$ (blue dashed line), 3.5 (red solid line), 4.0 (green dashed dotted line), and 4.5 a.u. (black short dashed line). The increase of the surface altitude Z appears to reduce the electron-transfer probability and shift the velocity thresholds for negative-ion conversion to larger values. This effect is attributed to the fact that the electron-transfer energy defect $\Delta E_{\rm ave}(Z,v)$ increases rapidly with Z.

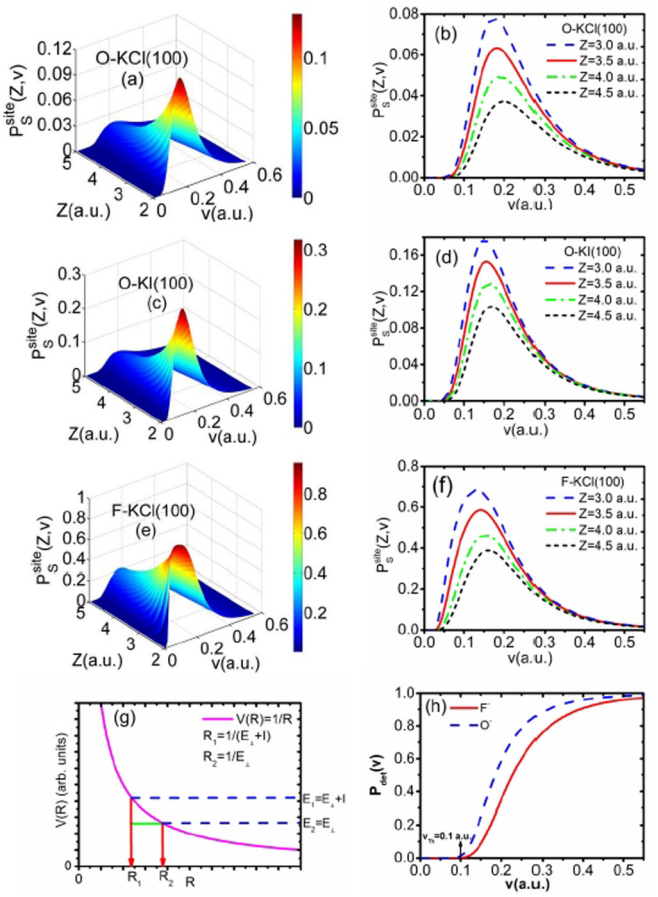

FIG. 6. (a) Probability of negative-ion conversion for a collision between $O^0_{\rm gas}$ and a $Cl^-_{\rm active\ site}$ at the KCl(100) surface in a single binary collision $O^0_{\rm gas} + Cl^-_{\rm active\ site} \rightarrow O^-_{\rm gas} + Cl^0_{\rm active\ site}$. The calculation is performed within the effective region S of $Cl^-_{\rm active\ site}$ at the KCl(100) surface. The figure displays the dependence of the probability $P^{\rm site}_{\rm S}(Z,v)$ on the projectile velocity v and the surface altitude Z as well as the projectile velocity dependence of the negative-ion conversion probability [$P^{\rm site}_{\rm S}(Z,v)$] in a single binary collision. Four representative values of the surface altitude, $Z = 3.0$ (blue dashed line), 3.5 (red solid line), 4.0 (green dashed dotted line), and 4.5 a.u. (black short dashed line), are displayed. Panels (c,e) and (d,f) are similar to panels (a,b), respectively, except they display cases of a single binary collision of $O^0_{\rm gas} + I^-_{\rm active\ site} \rightarrow O^-_{\rm gas} + I^0_{\rm active\ site}$ and $F^0_{\rm gas} + Cl^-_{\rm active\ site} \rightarrow F^-_{\rm gas} + Cl^0_{\rm active\ site}$. (g) Tunneling dynamics for the potential $V(R) = 1/R$. The classically allowed incoming and outgoing trajectories with the energies E_1 and E_2, respectively, are indicated by the blue dashed lines, and the tunneling is indicated by the green solid line. (h) Tunneling detachment probabilities for $O^-_{\rm gas} + Cl^-_{\rm site}$(or $I^-_{\rm site}$) $\rightarrow O^0_{\rm gas} + e^- + Cl^-_{\rm site}$(or $I^-_{\rm site}$) (blue dashed line) and $F^-_{\rm gas} + Cl^-_{\rm site} \rightarrow F^0_{\rm gas} + e^- + Cl^-_{\rm site}$ (red solid line).

For the $O^0_{\rm gas}$-KI(100) system, the single-collision negative-ion conversion probability $P^{\rm site}_{\rm S}(Z,v)$ resulting from $O^0_{\rm gas} + I^-_{\rm active\ site} \rightarrow O^-_{\rm gas} + I^0_{\rm active\ site}$ [Figs. 6(c) and 6(d)] is larger than that resulting from $O^0_{\rm gas} + Cl^-_{\rm active\ site} \rightarrow O^-_{\rm gas} + Cl^0_{\rm active\ site}$

[Figs. 6(a) and 6(b)] for the O^0_{gas}-KCl(100) case. This result is explained by the larger lattice constant of the KI crystal (a_{KI} = 13.34 a.u. [21]) compared to that of the KCl crystal (a_{KCl} = 11.9 a.u. [21]). As discussed in Sec. III A, a large lattice constant corresponds to a small PC-energy defect $\Delta E_{PC}(\mathbf{R})$ [which is observed in Fig. 2, where 0.5 eV $\leqslant \Delta E^{O\text{-}KCl}_{PC}(\mathbf{R}) - \Delta E^{O\text{-}KI}_{PC}(\mathbf{R}) \leqslant$ 0.8 eV for 2.0 a.u. $\leqslant Z \leqslant$ 5.0 a.u.]. Therefore, a pronounced large energy defect difference will directly lead to a more efficient electron-capture probability $P^{site}_{cap}(Z,v)$ for O^0_{gas}-KI(100) than for O^0_{gas}-KCl(100) and a larger single-collision negative-ion conversion probability $P^{site}_S(Z,v)$ of the O^0_{gas}-KI(100) case.

For F^0_{gas}-KCl(100), the single-collision $F^0_{gas} + Cl^-_{active\ site} \rightarrow F^-_{gas} + Cl^0_{active\ site}$ negative-ion conversion probability $P^{site}_S(Z,v)$ [Figs. 6(e) and 6(f)] is substantially greater than one order of magnitude larger than that of the single-collision $O^0_{gas} + Cl^-_{active\ site} \rightarrow O^-_{gas} + Cl^0_{active\ site}$ for the O^0_{gas}-KCl(100) case [Figs. 6(a) and 6(b)]. This result is attributed to the large electron-affinity difference of the neutral A^0_{gas} projectile ($\varepsilon_{F^-_{gas}} > 2\varepsilon_{O^-_{gas}}$) because (1) the large F^-_{gas} ion electron affinity leads to a significantly smaller electron-capture energy defect for F^0_{gas}-KCl(100) [see Figs. 5(e) and 5(d)], which naturally provides a larger electron-capture probability $P^{site}_{cap}(Z,v)$ than that of the O^0_{gas}-KCl(100) case; and (2) the large F^-_{gas} ion electron affinity also leads to a remarkably small detachment probability $P_{det}(v)$ of the outer loosely bound affinity electron as displayed in Fig. 6(h) (red solid line).

C. Comparison of the theoretical and experimental results

The negative-ion fraction $P(N)$ for an incident beam crossing N rows of surface ions obeys the differential equation $dP(N)/dN = [1 - P(N)]P^{row}_S(Z,v)$. Substituting this equation into the initial condition of $P(N = 0) = 0$ for a neutral projectile incidence, the final negative-ion fraction $P(N) = 1 - \exp[-P^{row}_S(Z,v)N]$is obtained. Combine the calculated $P^{row}_S(Z,v) = \frac{1}{2}\langle P^{site}_S(Z,v)\rangle_Z$ within Z values of 2.0 a.u. $\leqslant Z \leqslant$ 5.0 a.u.; see Fig. 7(d) [the contribution from the $Z >$ 5.0 a.u. range is negligible and can be found in Figs. 6(a)–6(f)]; the calculated final negative-ion conversion probabilities of the O^0_{gas} and F^0_{gas} atoms after grazing scattering from both the KCl(100) and KI(100) surfaces, which are displayed in Figs. 7(a)–7(c), with the available experimental data (black solid symbols) from Ref. [21]. Our approach provides a good description of the entire velocity range of the experimental data caused by increases of the average single-collision negative-ion conversion probability $\langle P^{site}_S(Z,v)\rangle_Z$ from the O^0_{gas}-KCl(100) to F^0_{gas}-KCl(100) cases [see Fig. 7(d)]. The final negative-ion yields increase from O^0_{gas}-KCl(100) to F^0_{gas}-KCl(100) as shown in Figs. 7(a)–7(c). Accurately determining the projectile-beam crossing number N related to the projectile trajectory calculation is beyond the scope of this work. Moreover, the attempts by Borisov *et al.* [14] to estimate the effective crossing number by $N \approx 2d/(a\tan\alpha)$ failed to determine d, where d represents the range from the closest approach distance to the surface that received the greatest contributions from the trajectories. While the same as in Ref. [22], one can roughly estimate the range of N by this

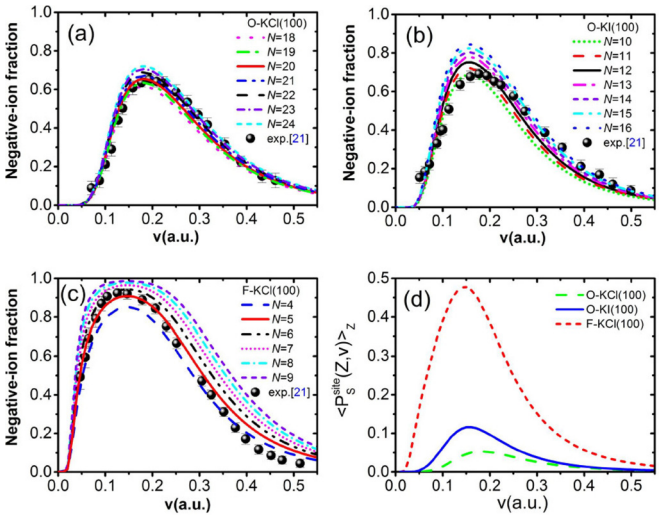

FIG. 7. (a–c) Comparison of the negative-ion yield versus the projectile velocity as measured for O^0_{gas}-KCl(100), O^0_{gas}-KI(100), and F^0_{gas}-KCl(100) [21] for an incidence angle $\alpha \approx 1^0$ as indicted by $\alpha = 1^0$. Black solid symbols in (a–c) represent experimental data [21] for three studied systems. The present theoretical results were displayed in (a–c) by different types of lines with the effective crossing number of $N_{O^0_{gas}\text{-}KCl} = 18 - 24$, $N_{O^0_{gas}\text{-}KI} = 10 - 16$, and $N_{F^0_{gas}\text{-}KCl} = 4 - 9$, respectively, for O^0_{gas}-KCl(100), O^0_{gas}-KI(100), and F^0_{gas}-KCl(100) systems. (d) The calculated results of $\langle P^{site}_S(Z,v)\rangle_Z$ for $P^{site}_S(Z,v)$ average over surface altitude Z values within the 2.0 a.u. $\leqslant Z \leqslant$ 5.0 a.u. range, where the green dashed line indicates O^0_{gas}-KCl(100); the blue solid line, O^0_{gas}-KI(100); the red short dashed line, F^0_{gas}-KCl(100).

formula within a typical range of $d <$ 2.0 a.u., hence, for the present three studied systems, $N_{O\text{-}KCl} < 19$, $N_{O\text{-}KI} < 17$, and $N_{F\text{-}KCl} < 19$, respectively. Here, to further show the effects of different values of effective crossing number N, $N_{O\text{-}KCl} = 18 - 24$, $N_{O\text{-}KI} = 10 - 16$, and $N_{F\text{-}KCl} = 4 - 9$ for O^0_{gas}-KCl(100), O^0_{gas}-KI(100), and F^0_{gas}-KCl(100) are, respectively, displayed in Figs. 7(a)–7(c) by different types of lines. The small increase of the final negative-ion fraction with the effective crossing number N implies a weak dependence on N. Additionally, for F^0_{gas}-KCl(100) comparing with both O^0_{gas}-KCl(100) and O^0_{gas}-KI(100) cases, the observed relatively larger increase of the negative-ion fraction $\Delta P = P(N+1) - P(N)$ with $\Delta N = 1$ resulted from the remarkable large average probability $\langle P^{site}_S(Z,v)\rangle_Z$ for the F^0_{gas}-KCl(100) case. Notably, the large difference of $N(N_{F\text{-}KCl} < N_{O\text{-}KI} < N_{O\text{-}KCl})$ may also be accounted for by the increase in the single-collision negative-ion conversion probability $P^{site}_S(Z,v)$ [or average probability $\langle P^{site}_S(Z,v)\rangle_Z$] from the O^0_{gas}-KCl(100) to F^0_{gas}-KCl(100) cases [see Figs. 6(a)–6(f) and Fig. 7(d)].

For $v \geqslant$ 0.3 a.u., the observed near-equal negative-ion formation fractions for the three studied systems shown in Figs. 7(a)–7(c) are caused by the dominant role of the negative ions formed in the detachment process in this velocity range and their (O^-_{gas} and F^-_{gas}) small difference in the

detachment probability $P_{\rm det}(v)$ [$\Delta P_{\rm det} = P_{\rm det}^{\rm O^-}(v \geqslant 0.3\,{\rm a.u.}) - P_{\rm det}^{\rm F^-}(v \geqslant 0.3{\rm a.u.}) \leqslant 0.1$; see Fig. 6(h)].

When compared to our previous study reported in Ref. [22], this work clearly reveals the following:

(1) the quantitative difference of the final negative-ion yields that result from the difference of the electron affinity between different projectile atoms; see Figs. 7(a) and 7(c). To be more specific, we show (I) the effect of the electron affinity on the electron-capture process which is due to its contribution to the electron-capture energy defect; see Fig. 2, which shows the point-charge energy defects difference $\Delta E_{\rm PC}^{\rm O\text{-}KCl} - \Delta E_{\rm PC}^{\rm F\text{-}KCl} = \varepsilon_{\rm F^-} - \varepsilon_{\rm O^-} = 1.94\,{\rm eV}$ of $O^0_{\rm gas}$-KI(100) compared with that of the $O^0_{\rm gas}$-KCl(100) case; (II) the effect of the difference of electron affinities ($\varepsilon_{\rm F^-} > 2\varepsilon_{\rm O^-}$) on the negative ions' detachment probabilities; see Fig. 6(h).

(2) the large influence of the final negative-ion yields by a small change in the lattice constant. This can be observed by comparing $O^0_{\rm gas}$-KCl(100) with $O^0_{\rm gas}$-KI(100) systems; a small change in lattice constant ($\Delta a = a_{\rm KI} - a_{\rm KCl} = 1.4\,{\rm a.u.}$) leads to an obvious change of the point-charge energy defect contribution to the final electron-capture energy defect (seen by $0.5\,{\rm eV} \leqslant \Delta E_{\rm PC}^{\rm KCl} - \Delta E_{\rm PC}^{\rm KI} \leqslant 0.8\,{\rm eV}$ (Fig. 2) relative to that of $O^0_{\rm gas}$-KI(100) [$1.7\,{\rm eV} \leqslant \Delta E_{\rm ave}^{\rm O\text{-}KI}(3.0\,{\rm a.u.} \leqslant Z \leqslant 4.0\,{\rm a.u.}, 0.08\,{\rm a.u.} \leqslant Z \leqslant 0.55\,{\rm a.u.}) \leqslant 2.3\,{\rm eV}$ (Fig. 5)] and $O^0_{\rm gas}$-KCl(100) [$2.7\,{\rm eV} \leqslant \Delta E_{\rm ave}^{\rm O\text{-}KCl}(3.0\,{\rm a.u.} \leqslant Z \leqslant 4.0\,{\rm a.u.}, 0.08\,{\rm a.u.} \leqslant v \leqslant 0.55\,{\rm a.u.}) \leqslant 3.3\,{\rm eV}$ (Fig. 5)], respectively). Therefore, it finally leads to an obvious difference of the negative-ion fractions for $O^0_{\rm gas}$-KCl(100) comparing with the $O^0_{\rm gas}$-KI(100) case; see Figs. 7(a) and 7(b).

(3) When comparing with electron affinity, the sensitivity of the lattice constant makes it play a dominate role in the final negative-ion formation.

IV. CONCLUSIONS

In this study, negative-ion conversions were performed for neutral O^0 and F^0 atoms under grazing scattering on both KCl and KI crystal surfaces over the entire velocity range. We found that the pronounced difference in the efficiency of negative-ion formation for F^0-KCl(100) and O^0-KCl(100) surfaces is attributed to large differences in the projectile electron affinity, which leads to (1) a larger electron-capture energy defect for O^0-KCl(100) than for F^0-KCl(100), and (2) a larger negative-ion affinity electron detachment probability formed for O^0-KCl(100) than for F^0-KCl(100). For O^0-KCl(100) comparing with O^0-KI(100) the difference can be explained by the differences in their lattice constants because the larger lattice constant of a KI crystal corresponds to a smaller PC electron-capture energy defect contribution to the final energy defect during the electron-capture reaction, which produces a larger electron-capture probability. This work will be useful in profound understanding of negative-ion conversion by neutral atoms grazing scattering from an ionic-crystal surface and its technical applications.

ACKNOWLEDGMENT

This work was supported by the National Natural Science Foundation of China (Grants No. 11175075 and No. 11404152).

[1] A. G. Borisov, D. Teillet-Billy, and P. Gauyacq, Phys. Rev. Lett. **68**, 2842 (1992).
[2] C. A. Keller, C. A. DiRubio, G. A. Kimmel, and B. H. Cooper, Phys. Rev. Lett. **75**, 1654 (1995).
[3] L. Guillemot and V. A. Esaulov, Phys. Rev. Lett. **82**, 4552 (1999).
[4] T. Hecht, H. Winter, A. G. Borisov, and J. P. Gauyacq, Phys. Rev. Lett. **84**, 2517 (2000).
[5] E. Sanchez, L. Guillemot, and V. A. Esaulov, Phys. Rev. Lett. **83**, 428 (1999).
[6] A. R. Canário and V. A. Esaulov, J. Chem. Phys. **124**, 224710 (2006).
[7] G. F. Liu, Z. Sroubek, and J. A. Yarmoff, Phys. Rev. Lett. **92**, 216801 (2004).
[8] E. R. Behringer, D. R. Andersson, B. H. Cooper, and J. B. Marston, Phys. Rev. B **54**, 14765 (1996).
[9] M. Maazouz, A. G. Borisov, V. A. Esaulov, J. P. Gauyacq, L. Guillemot, S. Lacombe, and D. Teillet-Billy, Phys. Rev. B **55**, 13869 (1997).
[10] J. Burgdörfer, E. Kupfer, and H. Gabriel, Phys. Rev. A **35**, 4963 (1987).
[11] A. G. Borisov, A. K. Kazansky, and J. P. Gauyacq, Phys. Rev. B **59**, 10935 (1999).
[12] Hi. Chakraborty, T. Niederhausen, and U. Thumm, Phys. Rev. A **69**, 052901 (2004).
[13] C. Auth, A. G. Borisov, and H. Winter, Phys. Rev. Lett. **75**, 2292 (1995).
[14] A. G. Borisov, V. Sidis, and H. Winter, Phys. Rev. Lett. **77**, 1893 (1996).
[15] S. Ustaze, R. Verucchi, S. Lacombe, L. Guillemot, and V. A. Esaulov, Phys. Rev. Lett. **79**, 3526 (1997).
[16] S. A. Deutscher, A. G. Borisov, and V. Sidis, Phys. Rev. A **59**, 4446 (1999).
[17] J. O. Lugo, E. C. Goldberg, E. A. Sánchez, and O. Grizzi, Phys. Rev. B **72**, 035432 (2005).
[18] H. Zhou, L. Chen, D. Feng, Y. Guo, M. Ji, G. Wang, W. Zhou, Y. Li, L. Zhao, and X. Chen, Phys. Rev. A **85**, 014901 (2012).
[19] P. Tiwald, S. Gräfe, J. Burgdörfer, and L. Wirtz, Nucl. Instrum. Methods Phys. Res., Sect. B **317**, 18 (2013).
[20] F. Labat, P. Baranek, and C. Adamo, J. Chem. Theory Comput. **4**, 341 (2008).
[21] C. Auth, A. Mertens, H. Winter, A. G. Borisov, and V. Sidis, Phys. Rev. A **57**, 351 (1998).
[22] H. Zhou, W. Zhou, M. Zhang, L. Zhou, Y. Ma, G. Wang, Y. Wu, B. Li, and X. Chen, Phys. Rev. A **93**, 062708 (2016).
[23] P. Wurz, J. Scheer, and M. Wieser, e-J. Surf. Sci. Nanotech. **4**, 394 (2006); M. Wieser, P. Wurz, K. Brüning, W. Heiland, Nucl. Instrum. Methods Phys. Res., Sect. B **192**, 370 (2002); F. W. Meyer, E. Galutschek, and M. Hotchkis, AIP Conf. Proc. **1099**, 308 (2009).

[24] *CRC Handbook of Chemistry and Physics*, 77th ed., edited by D. R. Linde (CRC Press, Boca Raton, FL, 1997).
[25] A. B. Kunz, Phys. Rev. B **12**, 5890 (1975); A. Zunger and A. J. Freeman, *ibid.* **16**, 2901 (1977); H. Tatewaki and E. Miyoshi, Surf. Sci. **327**, 129 (1995); G. K. Wertheim, J. E. Rowe, D. N. E. Buchanan, and P. H. Citrin, Phys. Rev. B **51**, 13675 (1995).
[26] A. G. Borisov and V. Sidis, Phys. Rev. B **56**, 10628 (1997).
[27] N. F. Mott and M. J. Littleton, Trans. Faraday Soc. **34**, 485 (1938); W. Beall Fowler, Phys. Rev. **151**, 657 (1966); G. D. Mahan, Phys. Rev. B **21**, 4791 (1980).
[28] A. G. Borisov, J. P. Gauyacq, V. Sidis, and A. K. Kazansky, Phys. Rev. B **63**, 045407 (2001).
[29] J. R. Tessman and A. H. Kahn, Phys. Rev. **92**, 890 (1953).
[30] P. M. Echenique and A. Howie, Ultramicroscopy **16**, 269 (1985); N. R. Arista, Phys. Rev. A **49**, 1885 (1994).
[31] E. D. Palik and W. R. Hunter, *Handbook of Optical Constants of Solids* (Academic Press, New York, 1985).
[32] J. H. Fertel and C. H. Perry, Phys. Rev. **184**, 874 (1969).